Aust. J. Phys., 1980, **33**, 73–90

Stress Enhancement of the *G* Line of Singly Ionized Zinc in Germanium

K. J. Duff,[A] *P. Fisher*[A] *and N. R. Butler*[B]

[A] Department of Physics, University of Wollongong, P. O. Box 1144, Wollongong, N.S.W. 2500.
[B] Defense Electronics Division, Electro-Optics Center, Honeywell Inc., 2 Forbes Road, Lexington, Massachusetts 02173, U.S.A.

Abstract

Predictions of the relative intensities of stress-induced components of the *D* and *G* lines of Zn^- in germanium are compared with the experimental results. Striking disagreement is obtained if interaction is permitted between both pairs of appropriate adjacent substates of the final states of these two transitions. However, if the Zn^- is allowed to be slightly displaced from the tetrahedral substitutional site and interaction is permitted between adjacent substates then the observations can be understood provided the displacement of the Zn^- from its substitutional site increases with stress and the very weak *G* line is split even at zero stress.

1. Introduction

The absorption spectrum of singly ionized zinc impurity in germanium has been studied in some detail previously (Rodriguez *et al.* 1972; Barra *et al.* 1973; Butler and Fisher 1976; hereinafter these references will be designated as Papers I, II and III respectively). Several features of the spectrum are well understood. A particular aspect of the spectrum is the spectacular growth of the *G* line (see Paper III) under uniaxial compression, and the origin of this has been qualitatively explained to be the result of stress-induced mixing of like-symmetry levels. Prior calculations (Chandrasekhar *et al.* 1973) have considered only mixing between adjacent stress-induced sublevels which would have crossed in the absence of their mutual interaction. It was recognized that this could only explain the growth of one but not both of the observed *G* components. In addition, only the ⟨111⟩ crystallographic orientation was analysed. The present paper extends the analysis to include all interactions between the sublevels of the final states of the *G* and *D* lines for both ⟨111⟩ and ⟨100⟩ directions of compression in an endeavour to obtain a quantitative correlation between the predicted and observed coupled states. The experimental results to be used are those of Paper III. It will be seen that the interaction between the *D* and *G* states is not sufficient to explain, quantitatively, the growth of the weaker *G* component. Accordingly, in Section 3 an additional mechanism is investigated, namely the displacement of the impurity ion from the substitutional tetrahedral site.

2. Interaction of Sublevels via the Strain Field

(*a*) *Theory*

Wavefunctions and Energies

A detailed study of the symmetries of the hole states of Zn^- in germanium and their splitting under uniaxial stress has been given in Paper I. The notation used therein (generalized where necessary) will be followed throughout the present paper.

We are concerned here with the interaction of hole states via the electrostatic potential of the strain field. The form this interaction takes is particularly illuminated by expressing this potential in a form which reflects the symmetry of the crystal, as was done in Paper I:

$$V = \sum_{rs} V_{rs}\varepsilon_{rs} = \{\tfrac{1}{3}(V_{xx}+V_{yy}+V_{zz})(\varepsilon_{xx}+\varepsilon_{yy}+\varepsilon_{zz})\}$$
$$+\{\tfrac{1}{6}(2V_{zz}-V_{xx}-V_{yy})(2\varepsilon_{zz}-\varepsilon_{xx}-\varepsilon_{yy})\}+\tfrac{1}{2}(V_{xx}-V_{yy})(\varepsilon_{xx}-\varepsilon_{yy})$$
$$+\{(V_{yz}+V_{zy})\varepsilon_{yz}+(V_{zx}+V_{xz})\varepsilon_{zx}+(V_{xy}+V_{yx})\varepsilon_{xy}\}, \qquad (1)$$

where

$$\varepsilon_{rs} = \tfrac{1}{2}(\partial u_r/\partial x_s + \partial u_s/\partial x_r).$$

The hole states of interest in this paper, in the absence of the stress, belong to the representation Γ_8 of the double point group $\overline{T}_d$ and are thus a fourfold degenerate manifold of states. Where two such manifolds interact, the interaction matrix is 8×8: the two 4×4 blocks on the diagonal were the subject of Paper I and, in general, these blocks contain the terms responsible for the lifting of the degeneracies as well as some overall shifts in energies; the two off-diagonal 4×4 blocks contain the interactions between the levels. The form of each of the 4×4 blocks is most easily constructed with the aid of the angular momentum matrices ($\hbar = 1$) for $J = 3/2$. Thus it has been shown in Paper I that

$$J^2 = J_x^2+J_y^2+J_z^2 = \tfrac{15}{4}I$$

belongs to Γ_1,

$$2J_z^2-J_x^2-J_y^2 = 3J_z^2-\tfrac{15}{4}I, \qquad \sqrt{3}(J_x^2-J_y^2)$$

belong to Γ_3, and

$$\{J_yJ_z\} = \tfrac{1}{2}(J_yJ_z+J_zJ_y), \quad \{J_zJ_x\} = \tfrac{1}{2}(J_zJ_x+J_xJ_z), \quad \{J_xJ_y\} = \tfrac{1}{2}(J_xJ_y+J_yJ_x)$$

belong to Γ_5. With the aid of these expressions the matrix of the potential (1) takes the form

$$[V] = a'_{ij}I(\varepsilon_{xx}+\varepsilon_{yy}+\varepsilon_{zz})$$
$$+b'_{ij}\big(\varepsilon_{xx}(J_x^2-\tfrac{5}{4}I)+\varepsilon_{yy}(J_y^2-\tfrac{5}{4}I)+\varepsilon_{zz}(J_z^2-\tfrac{5}{4}I)\big)$$
$$+(2d'_{ij}/\sqrt{3})\big(\{J_yJ_z\}\varepsilon_{yz}+\{J_zJ_x\}\varepsilon_{zx}+\{J_xJ_y\}\varepsilon_{xy}\big), \qquad (2)$$

where the block subscripts i and j take the values 1 and 2 for the upper states of the G and D transitions respectively. In this expression, the angular momentum matrix products have been combined with strain components of like symmetry so that the potential energy is manifestly a scalar quantity. The diagonal 4×4 blocks are given by $i = j$, while the off-diagonal blocks have $i \neq j$, with $a'_{ij} = a'^{*}_{ji}$, $b'_{ij} = b'^{*}_{ji}$ and $d'_{ij} = d'^{*}_{ji}$.

Let us assume that each of the on-diagonal 4×4 blocks has been diagonalized, and that the order of appearance of the diagonal elements in each of the two blocks has been determined by a common ordering of the corresponding eigenfunctions according to their symmetry. Then it follows that the off-diagonal 4×4 blocks have also been diagonalized since the potential can only mix states of like symmetry. We will designate the eigenfunctions of the on-diagonal 4×4 blocks $\Lambda_m^{(i)}$, where m takes four discreet values. It is a simple matter to rearrange the complete 8×8 matrix to take the form of four 2×2 matrices on the diagonal, one of which is

$$\begin{bmatrix} E_m^{(1)} & V_m \\ V_m^* & E_m^{(2)} \end{bmatrix}. \tag{3}$$

Thus the eigenfunctions for two interacting Γ_8 manifolds are (see Chandrasekhar *et al.* 1973)

$$\Lambda_m^{(+)} = \Lambda_m^{(1)} \sin\tfrac{1}{2}\theta_m - \exp(i\phi_m)\,\Lambda_m^{(2)} \cos\tfrac{1}{2}\theta_m, \tag{4a}$$

$$\Lambda_m^{(-)} = \Lambda_m^{(1)} \cos\tfrac{1}{2}\theta_m + \exp(i\phi_m)\,\Lambda_m^{(2)} \sin\tfrac{1}{2}\theta_m, \tag{4b}$$

where

$$R_m \exp(-i\phi_m)\sin\theta_m = -V_m, \qquad R_m = [\{\tfrac{1}{2}(E_m^{(1)} - E_m^{(2)})\}^2 + |V_m|^2]^{\frac{1}{2}}. \tag{5}$$

The corresponding energies are

$$E(\Lambda_m^{(+)}) = \tfrac{1}{2}(E_m^{(1)} + E_m^{(2)}) + R_m, \tag{6a}$$

$$E(\Lambda_m^{(-)}) = \tfrac{1}{2}(E_m^{(1)} + E_m^{(2)}) - R_m. \tag{6b}$$

Optical Intensities

The ground state for Zn^- in germanium is also a Γ_8 state which is energetically well displaced from the states considered above. We will designate the wavefunctions of the four components as $\Lambda_m^{(g)}$. The matrix elements of $\hat{Q}_k$, the operator for the component of the dipole moment along the direction of polarization, between the ground and excited states are

$$\langle \Lambda_m^{(+)} | \hat{Q}_k | \Lambda_n^{(g)} \rangle = \langle \Lambda_m^{(1)} | \hat{Q}_k | \Lambda_n^{(g)} \rangle \sin\tfrac{1}{2}\theta_m - \langle \Lambda_m^{(2)} | \hat{Q}_k | \Lambda_n^{(g)} \rangle \cos\tfrac{1}{2}\theta_m \exp(i\phi_m), \tag{7a}$$

$$\langle \Lambda_m^{(-)} | \hat{Q}_k | \Lambda_n^{(g)} \rangle = \langle \Lambda_m^{(1)} | \hat{Q}_k | \Lambda_n^{(g)} \rangle \cos\tfrac{1}{2}\theta_m + \langle \Lambda_m^{(2)} | \hat{Q}_k | \Lambda_n^{(g)} \rangle \sin\tfrac{1}{2}\theta_m \exp(i\phi_m), \tag{7b}$$

where n runs over the same four values as m. The intensities are proportional to the squares of the magnitudes of these matrix elements. If we assume that the phases of the wavefunctions $\Lambda_m^{(1)}$ and $\Lambda_m^{(2)}$ are not correlated (Chandrasekhar *et al.* 1973) so that an ensemble average of terms involving the product

$$\langle \Lambda_m^{(1)} | \hat{Q}_k | \Lambda_n^{(g)} \rangle \langle \Lambda_m^{(2)} | \hat{Q}_k | \Lambda_n^{(g)} \rangle$$

vanishes, we obtain for the relative intensities w

$$w_k(\Lambda_n^{(g)} \to \Lambda_m^{(+)}) = w_{nm,k}^{(1)} \sin^2\tfrac{1}{2}\theta_m + w_{nm,k}^{(2)} \cos^2\tfrac{1}{2}\theta_m, \tag{8a}$$

$$w_k(\Lambda_n^{(g)} \rightarrow \Lambda_m^{(-)}) = w_{nm,k}^{(1)} \cos^2 \tfrac{1}{2}\theta_m + w_{nm,k}^{(2)} \sin^2 \tfrac{1}{2}\theta_m, \tag{8b}$$

where

$$w_{nm,k}^{(i)} = |\langle \Lambda_m^{(i)} | \hat{Q}_k | \Lambda_n^{(g)} \rangle|^2.$$

If $\sin^2 \frac{1}{2}\theta_m$ is a monotonically increasing function of stress, these equations predict a progressively increasing transfer of intensity between the two final states $\Lambda_m^{(\pm)}$, and thus a weak spectral line with little or no intensity at zero stress may grow dramatically as stress is applied while another line diminishes simultaneously. It is, in principle, a simple matter to predict $\sin^2 \frac{1}{2}\theta_m$ from the observed energies of the spectral line: From equations (6),

$$R_m = \tfrac{1}{2}\{E(\Lambda_m^{(+)}) - E(\Lambda_m^{(-)})\} = \tfrac{1}{2}\{(E(\Lambda_m^{(+)}) - E(\Lambda_n^{(g)})) - (E(\Lambda_m^{(-)}) - E(\Lambda_n^{(g)}))\}. \tag{9}$$

Having found R_m, then from equations (5) we have

$$|V_m|^2 = R_m^2 - \{\tfrac{1}{2}(E_m^{(1)} - E_m^{(2)})\}^2 \tag{10}$$

and, finally,

$$\sin^2\theta_m = |V_m|^2 / R_m^2. \tag{11}$$

In practice, the application of the preceding recipe is complicated by the difficulty of locating accurately the positions of low intensity components, and the complexity of unfolding overlapping components. In addition, the energies $E_m^{(1)}$ and $E_m^{(2)}$ are not measured directly, but must be computed by a curve-fitting procedure. From equations (6),

$$E(\Lambda_m^{(+)}) - E(\Lambda_m^{(-)}) = 2R_m = \left(E_m^{(1)} - E_m^{(2)}\right)\left(1 + \frac{4|V_m|^2}{(E_m^{(1)} - E_m^{(2)})^2}\right)^{\frac{1}{2}}, \tag{12a}$$

$$= E_m^{(1)} - E_m^{(2)} + \frac{2|V_m|^2}{E_m^{(1)} - E_m^{(2)}} + \ldots. \tag{12b}$$

Since $|V_m|$ is proportional to stress and $E_m^{(1)} - E_m^{(2)}$, while linear in stress, contains a constant term, the term in $|V_m|^2$ is quadratic in stress, so that the linear part of the expansion of $E(\Lambda_m^{(+)}) - E(\Lambda_m^{(-)})$ as a function of stress for small stress gives $E_m^{(1)} - E_m^{(2)}$ directly. Thus

$$|V_m|^2 = \tfrac{1}{4}[(E(\Lambda_m^{(+)}) - E(\Lambda_n^{(g)})) - (E(\Lambda_m^{(-)}) - E(\Lambda_n^{(g)}))]^2$$

$$- \tfrac{1}{4}\{[(E(\Lambda_m^{+}) - E(\Lambda_n^{(g)})) - (E(\Lambda_m^{-}) - E(\Lambda_n^{(g)}))]_{LP}\}^2, \tag{13}$$

where the subscript LP denotes the linear part.

It should be noted that, in the above, the results are independent of whether the separation of the two interacting levels is initially decreasing or increasing, i.e. it is not a requirement that the levels cross in the absence of interaction.

Application to Stress in [111] *Direction*

As in Paper I, the strain components for an applied compressive force $\boldsymbol{F}$ along the [111] direction are

$$\varepsilon_{xx} = \varepsilon_{yy} = \varepsilon_{zz} = \tfrac{1}{3}T(s_{11}+2s_{12}), \qquad \varepsilon_{xy} = \varepsilon_{yz} = \varepsilon_{zx} = \tfrac{1}{6}Ts_{44},$$

where T is the stress and is negative for compression, and the s_{ij}'s are the elastic compliance coefficients. Equation (2) becomes

$$[V] = \{a'_{ij}(s_{11}+2s_{12})-(5d'_{ij}/8\sqrt{3})s_{44}\}TI+(d'_{ij}/6\sqrt{3})(J_x+J_y+J_z)^2Ts_{44}.$$

On diagonalization of the 4×4 on-diagonal blocks, the functions $\Lambda^{(i)}_m$ are found to fall into two Kramers doublets (for a given i) which are designated $(\Lambda^{(i)}_{3/2}, \Lambda^{(i)}_{-3/2})$ and $(\Lambda^{(i)}_{1/2}, \Lambda^{(i)}_{-1/2})$, and their energies are

$$E(\Lambda^{(i)}_{\pm3/2}) = E^{(i)}_{(0)}+a'_{ii}(s_{11}+2s_{12})T+(d'_{ii}/2\sqrt{3})s_{44}T, \tag{14a}$$

$$E(\Lambda^{(i)}_{\pm1/2}) = E^{(i)}_{(0)}+a'_{ii}(s_{11}+2s_{12})T-(d'_{ii}/2\sqrt{3})s_{44}T, \tag{14b}$$

where $E^{(i)}_{(0)}$ is the zero-stress energy of the manifold of states designated by i. As a consequence of this, the off-diagonal elements in the matrix (3) are related to one another as follows:

$$V_{3/2} = V^*_{-3/2} = a'_{12}T(s_{11}+2s_{12})+(d'_{12}/2\sqrt{3})Ts_{44}, \tag{15a}$$

$$V_{1/2} = V^*_{-1/2} = a'_{12}T(s_{11}+2s_{12})-(d'_{12}/2\sqrt{3})Ts_{44}. \tag{15b}$$

For the transitions from the ground states as described by equations (8) we therefore have only two distinct parameters θ_m, which we can designate $\theta_{3/2}$ and $\theta_{1/2}$.

Using equations (8), we can tabulate the relative intensities of the various stress-induced components of the original absorption lines. These are given in Table 1*a*, where it has been more convenient to designate $\theta_{1/2}$ and $\theta_{3/2}$ by θ' and θ respectively and to replace the parameters $w^{(i)}_{nm,k}$ with the equivalent expressions as used in Paper I and by Chandrasekhar *et al.* (1973); for example,

$$w^{(i)}_{1/2,3/2,\perp} = N_i(\tfrac{1}{2}-\tfrac{1}{4}u_i) \qquad \text{while} \qquad w^{(i)}_{3/2,1/2,\parallel} = 0.$$

In these examples, the two directions of polarization correspond to the electric vector $\boldsymbol{E}$ of the radiation being either perpendicular ($\perp$) or parallel ($\parallel$) to the applied force $\boldsymbol{F}$.

It is interesting to note that if in Table 1*a* transitions of the same type, e.g. $\Gamma_4 \rightarrow \Gamma_{5+6}$ of G and D for perpendicular polarization, are added together then the resultant is independent of $\theta_{1/2}$ or $\theta_{3/2}$. Further, if the experimental values of u_1, u_2, N_1 and N_2 are inserted into the resulting expressions it is found that the combination $N_1u_1+N_2u_2$ is *independent of the impurity and host crystal.* For Zn^- in germanium, $N_1 \approx 0$, $N_2 \approx 1{\cdot}0$ and $u_2 \approx 0{\cdot}23$ (see Papers II and III where u_1 is written as u_D) while, for boron in silicon, $N_1 \approx 0{\cdot}17$, $N_2 \approx 0{\cdot}83$, $u_1 \approx 0{\cdot}9$ and $u_2 \approx 0{\cdot}1$ (see Chandrasekhar *et al.* 1973). For these cases then $N_1u_1+N_2u_2$ is $0{\cdot}230$ and $0{\cdot}236$ respectively, thus giving rise to the above generalization. This presumably has its origin in the parent states from which these states are derived.

Table 1. Calculated relative intensities of stress-induced components of transitions for Zn^- in germanium

The results are for transitions from a Γ_8 ground state to two interacting adjacent Γ_8 states for (*a*) $\boldsymbol{F} \parallel \langle 111 \rangle$ and (*b*) $\boldsymbol{F} \parallel \langle 001 \rangle$. For clarity of presentation, $\theta_{1/2}$ and $\theta_{3/2}$ in the text are given here as θ' and θ respectively. The parameters N_1, N_2 and u_2 are 0, 1 and 0·23 respectively, for Zn^- in germanium (see Papers II and III)

Transition	Spectral line	Relative intensities of components $\boldsymbol{E} \parallel \boldsymbol{F}$	$\boldsymbol{E} \perp \boldsymbol{F}$
		(*a*) $\boldsymbol{F} \parallel \langle 111 \rangle$	
$\Gamma_4 \rightarrow \Gamma_4$	G_3	$N_1(\frac{1}{2}-\frac{1}{2}u_1)\cos^2\frac{1}{2}\theta' + N_2(\frac{1}{2}-\frac{1}{2}u_2)\sin^2\frac{1}{2}\theta'$	$\frac{1}{2}N_1 u_1 \cos^2\frac{1}{2}\theta' + \frac{1}{2}N_2 u_2 \sin^2\frac{1}{2}\theta'$
$\Gamma_4 \rightarrow \Gamma_{5+6}$	G_4	0	$N_1(\frac{1}{2}-\frac{1}{4}u_1)\cos^2\frac{1}{2}\theta + N_2(\frac{1}{2}-\frac{1}{4}u_2)\sin^2\frac{1}{2}\theta$
$\Gamma_{5+6} \rightarrow \Gamma_4$	G_1	0	$N_1(\frac{1}{2}-\frac{1}{4}u_1)\cos^2\frac{1}{2}\theta' + N_2(\frac{1}{2}-\frac{1}{4}u_2)\sin^2\frac{1}{2}\theta'$
$\Gamma_{5+6} \rightarrow \Gamma_{5+6}$	G_2	$N_1(\frac{1}{2}+\frac{1}{2}u_1)\cos^2\frac{1}{2}\theta + N_2(\frac{1}{2}+\frac{1}{2}u_2)\sin^2\frac{1}{2}\theta$	0
$\Gamma_4 \rightarrow \Gamma_4$	D_4	$N_1(\frac{1}{2}-\frac{1}{2}u_1)\sin^2\frac{1}{2}\theta' + N_2(\frac{1}{2}-\frac{1}{2}u_2)\cos^2\frac{1}{2}\theta'$	$\frac{1}{2}N_1 u_1 \sin^2\frac{1}{2}\theta' + \frac{1}{2}N_2 u_2 \cos^2\frac{1}{2}\theta'$
$\Gamma_4 \rightarrow \Gamma_{5+6}$	D_3	0	$N_1(\frac{1}{2}-\frac{1}{4}u_1)\sin^2\frac{1}{2}\theta + N_2(\frac{1}{2}-\frac{1}{4}u_2)\cos^2\frac{1}{2}\theta$
$\Gamma_{5+6} \rightarrow \Gamma_4$	D_2	0	$N_1(\frac{1}{2}-\frac{1}{4}u_1)\sin^2\frac{1}{2}\theta' + N_2(\frac{1}{2}-\frac{1}{4}u_2)\cos^2\frac{1}{2}\theta'$
$\Gamma_{5+6} \rightarrow \Gamma_{5+6}$	D_1	$N_1(\frac{1}{2}+\frac{1}{2}u_1)\sin^2\frac{1}{2}\theta + N_2(\frac{1}{2}+\frac{1}{2}u_2)\cos^2\frac{1}{2}\theta$	0
		(*b*) $\boldsymbol{F} \parallel \langle 001 \rangle$	
$\Gamma_6 \rightarrow \Gamma_6$	G_2	0	$\frac{3}{8}(N_1 u_1 \cos^2\frac{1}{2}\theta + N_2 u_2 \sin^2\frac{1}{2}\theta)$
$\Gamma_6 \rightarrow \Gamma_7$	G_1	$N_1(\frac{1}{2}-v_1)\cos^2\frac{1}{2}\theta' + N_2(\frac{1}{2}-v_2)\sin^2\frac{1}{2}\theta'$	$\frac{1}{2}N_1(1-\frac{3}{4}u_1+v_1)\cos^2\frac{1}{2}\theta' + \frac{1}{2}N_2(1-\frac{3}{4}u_2+v_2)\sin^2\frac{1}{2}\theta'$
$\Gamma_7 \rightarrow \Gamma_6$	G_4	$N_1(\frac{1}{2}+v_1)\cos^2\frac{1}{2}\theta + N_2(\frac{1}{2}+v_2)\sin^2\frac{1}{2}\theta$	$\frac{1}{2}N_1(1-\frac{3}{4}u_1-v_1)\cos^2\frac{1}{2}\theta + \frac{1}{2}N_2(1-\frac{3}{4}u_2-v_2)\sin^2\frac{1}{2}\theta$
$\Gamma_7 \rightarrow \Gamma_7$	G_3	0	$\frac{3}{8}(N_1 u_1 \cos^2\frac{1}{2}\theta' + N_2 u_2 \sin^2\frac{1}{2}\theta')$
$\Gamma_6 \rightarrow \Gamma_6$	D_1	0	$\frac{3}{8}(N_1 u_1 \sin^2\frac{1}{2}\theta + N_2 u_2 \cos^2\frac{1}{2}\theta)$
$\Gamma_6 \rightarrow \Gamma_7$	D_2	$N_1(\frac{1}{2}-v_1)\sin^2\frac{1}{2}\theta' + N_2(\frac{1}{2}-v_2)\cos^2\frac{1}{2}\theta'$	$\frac{1}{2}N_1(1-\frac{3}{4}u_1+v_1)\sin^2\frac{1}{2}\theta' + \frac{1}{2}N_2(1-\frac{3}{4}u_2+v_2)\cos^2\frac{1}{2}\theta'$
$\Gamma_7 \rightarrow \Gamma_6$	D_3	$N_1(\frac{1}{2}+v_1)\sin^2\frac{1}{2}\theta + N_2(\frac{1}{2}+v_2)\cos^2\frac{1}{2}\theta$	$\frac{1}{2}N_1(1-\frac{3}{4}u_1-v_1)\sin^2\frac{1}{2}\theta + \frac{1}{2}N_2(1-\frac{3}{4}u_2-v_2)\cos^2\frac{1}{2}\theta$
$\Gamma_7 \rightarrow \Gamma_7$	D_4	0	$\frac{3}{8}(N_1 u_1 \sin^2\frac{1}{2}\theta' + N_2 u_2 \cos^2\frac{1}{2}\theta')$

Application to Stress in [001] *Direction*

Again following Paper I, for a force $\boldsymbol{F}$ applied in the [001] direction, the components of strain are $\varepsilon_{xx} = \varepsilon_{yy} = s_{12}T$, $\varepsilon_{zz} = s_{11}T$ and $\varepsilon_{xy} = \varepsilon_{yz} = \varepsilon_{zx} = 0$. The interaction matrix of equation (2) becomes,

$$[V] = a'_{ij}(s_{11}+2s_{12})TI + b'_{ij}(s_{11}-s_{12})T(J_z^2-\tfrac{5}{4}I).$$

The diagonalization of each on-axis block produces two Kramers doublets designated $(\psi^{(i)}_{3/2}, \psi^{(i)}_{-3/2})$ and $(\psi^{(i)}_{1/2}, \psi^{(i)}_{-1/2})$, with energies

$$E(\psi^{(i)}_{\pm 3/2}) = E^{(i)}_{(0)} + a'_{ii}(s_{11}+2s_{12})T + b'_{ii}(s_{11}-s_{12})T, \tag{16a}$$

$$E(\psi^{(i)}_{\pm 1/2}) = E^{(i)}_{(0)} + a'_{ii}(s_{11}+2s_{12})T - b'_{ii}(s_{11}-s_{12})T. \tag{16b}$$

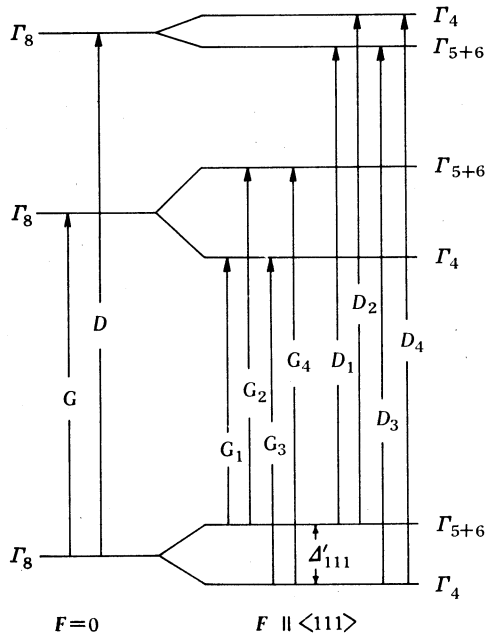

Fig. 1. Energy levels and transitions for the D and G excitation lines of a single acceptor in germanium for a compressive force F applied along a ⟨111⟩ direction.

The off-axis matrix elements are

$$V_{3/2} = a'_{12}(s_{11}+2s_{12})T + b'_{12}(s_{11}-s_{12})T, \tag{17a}$$

$$V_{1/2} = a'_{12}(s_{11}+2s_{12})T - b'_{12}(s_{11}-s_{12})T, \tag{17b}$$

with $V_{3/2} = V^*_{-3/2}$ and $V_{1/2} = V^*_{-1/2}$. Once again we have only two parameters θ_m and we again designate them $\theta_{3/2}$ and $\theta_{1/2}$. The relative intensities in this case are given in Table 1*b*. As is the case in general, an additional parameter v occurs in the expressions for w. This is fully discussed in Paper I.

Calculations for the relative intensities for F parallel to ⟨110⟩ have not been carried out. From an examination of Table XVIII in Paper I, it is seen that the expressions for these intensities, even in the absence of interactions between sublevels, are lengthy and cumbersome and in any case contribute nothing further than the information already obtained for the other two directions. Introduction of interactions between sublevels for the ⟨110⟩ case would produce expressions that would be even more cumbersome.

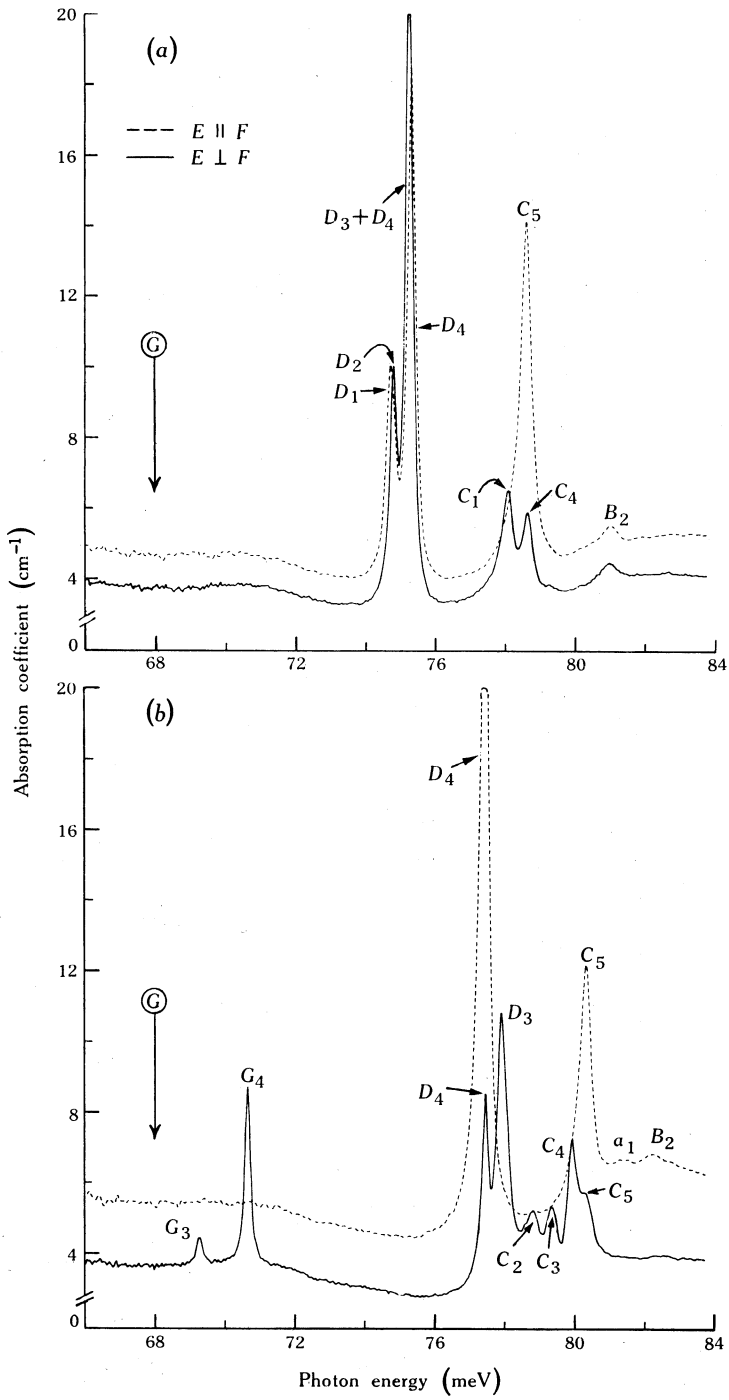

Fig. 2. Excitation spectra of Zn^- in germanium (Sample No. 436–4A) for ***F*** parallel to ⟨111⟩ at stresses of (*a*) 0·276 kbar and (*b*) 1·93 kbar; liquid helium was used as coolant. The position indicated by the encircled *G* is the zero-stress energy of the *G* line. (Note that 1 kbar ≡ 0·1 GPa.)

(b) Experimental results

The levels and transitions of interest are shown schematically in Fig. 1 for $\boldsymbol{F}$ parallel to $\langle 111 \rangle$. Most of the experimental data for the stress-induced behaviour of the absorption spectrum of Zn^- in germanium are reported in Paper III. However, some unpublished examples are given in Figs 2*a* and 2*b* for $\boldsymbol{F}$ parallel to $\langle 111 \rangle$; it is the behaviour of the D and G components with which we are concerned here. Further processing of the published and unpublished data has been performed to permit quantitative comparisons to be made between the experiment and theory.

Before making any detailed quantitative comparisons, it is clear that the results given in Table 1 for the G_3 components are not compatible with experiment. The strengths of the G_3 components, $G_3^{\parallel}$ and $G_3^{\perp}$ (radiation polarized parallel and perpendicular respectively to $\boldsymbol{F}$), are due to the sine-squared terms since we have $N_1 \approx 0$ (see Paper III). As specified above, the value of u_2 is 0·23 and thus $G_3^{\parallel}$ is predicted to be about three times as strong as $G_3^{\perp}$, whereas, experimentally, $G_3^{\parallel}$ is extremely weak, if observed at all.

Comparisons between the perpendicular components $G_3^{\perp}$, $G_4^{\perp}$, $D_3^{\perp}$ and $D_4^{\perp}$ require the θ values to be calculated. The values of $\theta_{3/2}$ and $\theta_{1/2}$ are obtained by the use of equations (9)–(13), and fits to the experimental data to give the stress dependence at low stresses of the energies of the components. The fits obtained for the D components were modified very slightly so that the energy differences of D_4 and D_2 and of D_3 and D_1 were the same, namely the ground state splitting, and the energy differences of D_4 and D_3 and of D_2 and D_1 were the same, namely the excited state splitting. Such modifications to the fits for the G components could not be made since G_1 and G_2 were not observed.

The experimental intensities for $D_3^{\perp}$ and $G_4^{\perp}$ are shown in Fig. 3 (curves D_3^o and G_4^o respectively). For stresses below $\sim$1·5 kbar (0·15 GPa), the $D_3^{\perp}$ and $D_4^{\perp}$ components were not separately resolved, and hence the combined intensities of $D_3^{\perp}$ and $D_4^{\perp}$ are plotted (curve D_{34}^o). Because it is subsequently useful, the plot of the combined intensities has been extended over the full range of the measurements.

In Fig. 3, the intensities have been determined from the areas of the absorption lines using the method of weighing 'cut-outs' of the absorption lines; a spectrum recorded at low stress (see Fig. 2*a*) was used for background subtraction. Where components overlapped, a graphical reconstruction was used to 'peel' each component away from the rest. The intensities presented for G_4 in Fig. 3 are larger than those given in Paper III due to the different methods used to evaluate the areas of the peaks. In Fig. 8 of Paper III, the intensities of G_4 were obtained from the half-widths and peak heights. The procedure used here will produce intensities which are somewhat more dependent upon the assumed background absorption than that of Paper III, particularly for weak components. However, it does have the advantage that it permits a more realistic evaluation of intensities of overlapping components and better absolute values of intensities.

Under uniaxial stress, the Γ_8 ground state splits into two sublevels (see Fig. 1). The splitting for $\boldsymbol{F}$ parallel to $\langle 111 \rangle$ is given experimentally by $\Delta'_{111} = 1{\cdot}95\,T$ meV, where T is in kilobars. As a consequence, the upper ground state is progressively depopulated with stress and the lower ground state has its population enhanced. For the temperature at which the experiments were performed ($\sim$7 K), the upper ground state is essentially unpopulated at stresses above $\sim$1·5 kbar. It is this effect

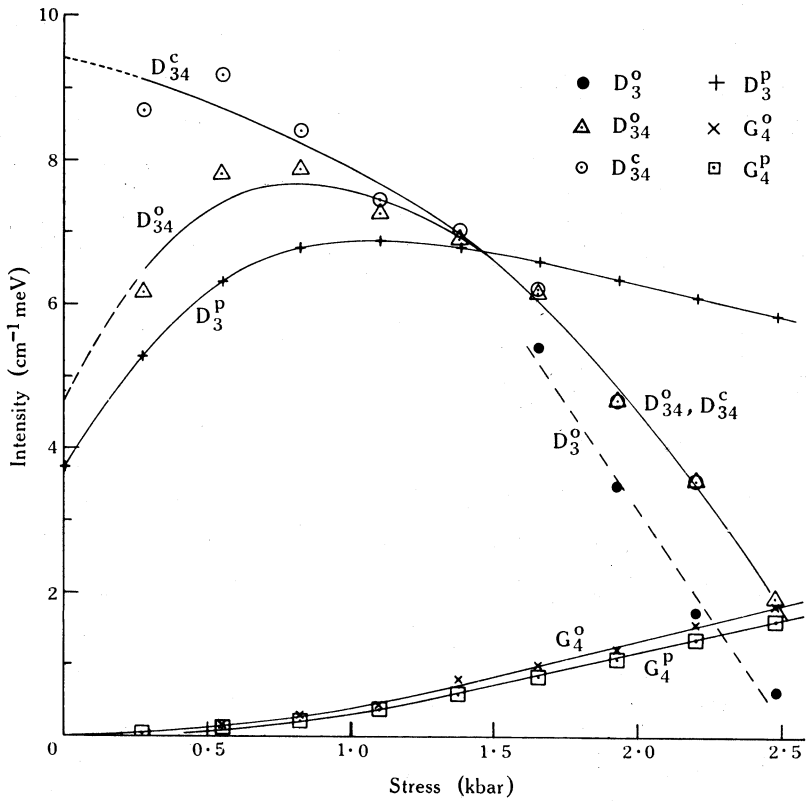

Fig. 3. Experimental and predicted intensities for $D_3^{\perp}$, $D_3^{\perp}+D_4^{\perp}$ and $G_4^{\perp}$ for F parallel to ⟨111⟩:

D_3^o, measured intensities for $D_3^{\perp}$;

D_{34}^o, combined measured intensities of $D_3^{\perp}$ and $D_4^{\perp}$;

D_{34}^c, combined intensities of $D_3^{\perp}$ and $D_4^{\perp}$ compensated to remove the effects of a varying population of the lower ground state consequent on a temperature of 7 K and a stress-dependent splitting of the ground state;

D_3^p, intensity of $D_3^{\perp}$ predicted from the appropriate expression in Table 1, together with appropriate temperature-compensation factors;

G_4^o, measured intensities of $G_4^{\perp}$;

G_4^p, intensities of $G^{\perp}$ predicted from the appropriate expression in Table 1, together with the appropriate temperature-compensation factors.

which causes the components D_1 and D_2 to become progressively weaker and eventually to disappear, as is seen by comparison of the spectra shown in Figs 2*a* and 2*b*. Above $\sim 1{\cdot}5$ kbar, the lower ground state population is essentially constant. In terms of the theory this means that the parameters N_1 and N_2 are essentially constant in the higher range of stresses. In the lower range of stresses, N_1 and N_2 must be reduced by the appropriate Boltzmann factors. The value of N_2 to be used in the upper range can be determined by compensating the measured combined intensities of D_3 and D_4 with the appropriate Boltzmann factors and extrapolating back to zero stress. This is shown in Fig. 3, the intercept of the compensated curve D_{34}^c on the intensity axis of $9{\cdot}4$ meV cm^{-1} yielding $N_2 = 16{\cdot}9$ meV cm^{-1}. This is

based on a sample temperature of 7 K; it should be noted that if the sample temperature is different from the assumed value by ± 1 K then the above intercept differs from 9·4 by $\pm 0{\cdot}8$ with proportionate changes in N_2. The computed value of N_2 together with the values of $\theta_{3/2}$ and $\theta_{1/2}$ permit the evaluation of the intensities of all components listed in Table 1, with the previous assumption that $N_1 = 0$. In Fig. 3, the predicted intensities of $D_3^{\perp}$ and $G_4^{\perp}$ are plotted (curves D_3^p and G_4^p). In Fig. 4 are shown the experimental and predicted intensities for $G_3^{\perp}$; for ease of comparison also the values for $G_4^{\perp}$ plotted in Fig. 3 have been replotted in Fig. 4. Note that the scale for the predicted values of $G_3^{\perp}$ is 10 times that of the experimental values.

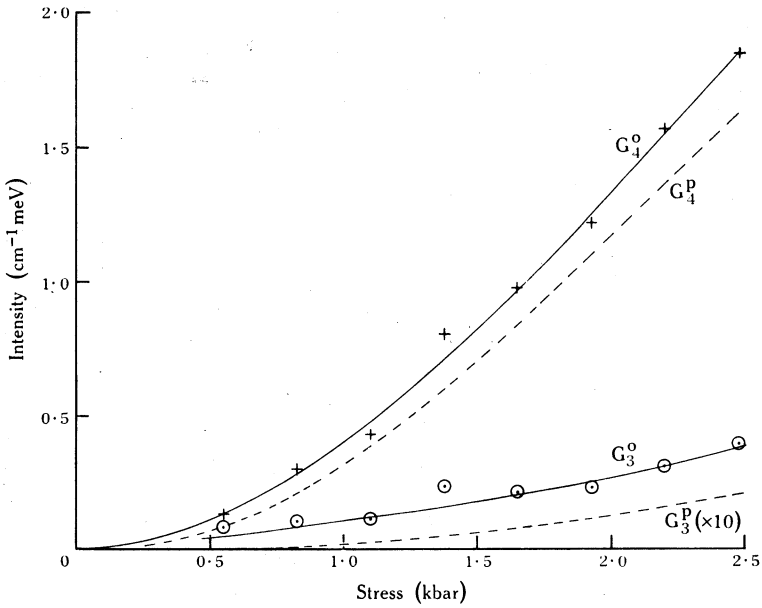

Fig. 4. Experimental and predicted intensities of $G_3^{\perp}$ and $G_4^{\perp}$ for F parallel to ⟨111⟩. For comparison, the two curves of Fig. 3 for $G_4^{\perp}$ are repeated here. The solid lines G_3^o and G_4^o depict the measured data for $G_3^{\perp}$ and $G_4^{\perp}$ while the dashed lines G_3^p and G_4^p are the corresponding predictions from the expressions in Table 1. It should be noted that the predicted intensities for the $G_3^{\perp}$ component have been scaled by a factor of 10 in order to display these results clearly.

It is seen from Fig. 3 that there is good agreement between the observed and predicted values of $G_4^{\perp}$. This is somewhat surprising since the source of the intensity of G_4 is the D_3 component which experimentally is much weaker than that predicted. The dramatic difference between the observed and predicted values of $D_3^{\perp}$ would appear to be due to a further interaction, possibly with the excited states of the C line (see Paper III). Our model for the determination of the θ values presumes no further interaction than that with the G states. If the presumed C–D interaction were absent the curvature of the curve for the stress dependence of the energies of the D components (see Fig. 9, Paper III) would be greater than that observed thus producing larger θ's and hence greater enhancement of the G components. Fig. 4 reveals that the predicted $G_3^{\perp}$ component is typically weaker than that observed by a factor of ~ 20.

Of the concrete predictions of the effect of interaction between D and G levels, only the intensity of the $G_4^{\perp}$ has been confirmed and even then the agreement appears to be fortuitous. There are three distinct contradictions between the experimental results and the predictions, namely the relative intensities of $G_3^{\parallel}$ and $G_3^{\perp}$ and the absolute intensities of $D_3^{\perp}$ and of $G_3^{\perp}$. It is concluded that this interaction is not the sole mechanism giving rise to the G components.

3. Zn^- in a Non-tetrahedral Site

In this section, we explore the possibility that the negative ion is not located at a lattice site, but is slightly displaced in the [100] direction. The expected consequences of a *small* displacement are:

(i) a mixing of the wavefunctions within each manifold of states describing each multiplet level and a consequent transfer of optical intensities between levels;

(ii) a zero-stress splitting of some otherwise degenerate levels;

(iii) almost no mixing between energetically well-separated states, provided the displacement is small enough.

Effects (i) and (ii) may be significant for some groups of levels but not for others, because the magnitudes of the effects depend on the matrix elements of the operator describing the alteration of the field by the displacement and these matrix elements may differ substantially between the different manifolds of states. There is some evidence that 'substitutional' aluminium in silicon does not occupy a tetrahedral site but has trigonal symmetry, being displaced very slightly along a $\langle 111 \rangle$ direction (see Chandrasekhar *et al.* 1975).

We model the alteration of the field of the ion by adding to all previously considered fields the field of a dipole located at the lattice position oriented antiparallel to the displacement; this, of course, represents the dominant correction term in a multipole expansion about the lattice site, of the field of the displaced ion, it being reasonable to neglect quadrupole and higher order terms. We have chosen a $\langle 100 \rangle$ direction as the likely direction of movement by inspection of a crystal model and available space considerations. Although other directions of movement might equally well be considered, our choice suffices for a consideration of the plausibility of the conjecture of off-centre movement. Since this is intended as an exploratory calculation we also make the following assumptions:

(iv) as the intensity of the G_3 line could not be explained by the mechanism considered in Section 2*a* above, we are justified in setting the appropriate coupling matrix elements $V_{1/2}$ to zero;

(v) the zero-stress intensities of the G components are zero, that is, $w^{(1)}_{nm,k} = 0$ in equations (8);

(vi) since mixing of ground level states could not, by itself, produce any intensity in the G_3 components, we will neglect the effect of the off-centre movement on ground states, recognizing that, for the components with significant zero-stress intensities, those we calculate could perhaps be modified if there is in fact some ground state mixing as a result of the off-centre movement.

(*a*) *Theory*

The Hamiltonian for the hole–ion system is

$$H = H_0 + H_{\text{int}} + H_{\text{dp}}, \tag{18}$$

where H_0 contains all terms considered in Paper I, and specifically the potential of the strain field, but, however, excludes the interaction between the G_4 and D_3 levels, which is incorporated in H_{int}. Thus $H_0 + H_{\text{int}}$ contains all terms considered by Chandrasekhar *et al.* (1973). The dipole contribution is represented in equation (18) by H_{dp}. We use as basis functions the eigenfunctions of H_0, namely $\Lambda_m^{(i)}$, as used in the matrix (3) and listed in Paper I. In this case H_0 is diagonal and H_{int} is everywhere zero, except for the matrix elements $V_{3/2}$ coupling the $\Lambda_{\pm 3/2}^{(1)}$ states with the $\Lambda_{\pm 3/2}^{(2)}$ states. Paper I lists the form of the matrices for the components of the dipole moment operator for three orthogonal directions, and these are easily combined to construct the matrix for a dipole oriented in the [100] direction. According to our assumption (iii) above, we are not concerned with matrix elements of the dipole moment operator connecting states in different manifolds. Thus, we may append a superscript 1 or 2 to H_{dp} to indicate an on-diagonal 4×4 submatrix derived from the G or D manifolds, and in this case

$$H_{\text{dp}}^{(i)} = \begin{bmatrix} -\alpha_i & \alpha_i & \mathrm{i}\alpha_i & 0 \\ \alpha_i & \alpha_i & 0 & -\mathrm{i}\alpha_i \\ -\mathrm{i}\alpha_i & 0 & \alpha_i & \alpha_i \\ 0 & \mathrm{i}\alpha_i & \alpha_i & -\alpha_i \end{bmatrix}. \tag{19}$$

The parameters α_i ($i = 1, 2$) are real and are proportional to the dipole moment, and are therefore simply proportional to the displacement of the ion from the lattice position.

We now diagonalize $H_0 + H_{\text{int}}$ by transforming to the set of states

$$\Lambda_{3/2}^{(+)},\ \Lambda_{1/2}^{(2)},\ \Lambda_{-1/2}^{(2)},\ \Lambda_{-3/2}^{(+)},\ \Lambda_{3/2}^{(-)},\ \Lambda_{1/2}^{(1)},\ \Lambda_{-1/2}^{(1)},\ \Lambda_{-3/2}^{(-)}.$$

This procedure recognizes the importance of the coupling of the $\Lambda_{\pm 3/2}^{(1)}$ states with the $\Lambda_{\pm 3/2}^{(2)}$ states through the strain field by treating it exactly. The form of H is then

$$H = \begin{bmatrix} E_{3/2}^{(+)} & -\lambda_2^* & -\mathrm{i}\lambda_2^* & 0 & 0 & \mu_1 & \mathrm{i}\mu_1 & 0 \\ -\lambda_2 & E_{1/2}^{(2)} & 0 & \mathrm{i}\lambda_2^* & \mu_2 & 0 & 0 & -\mathrm{i}\mu_2^* \\ \mathrm{i}\lambda_2 & 0 & E_{1/2}^{(2)} & -\lambda_2^* & -\mathrm{i}\mu_2 & 0 & 0 & \mu_2^* \\ 0 & -\mathrm{i}\lambda_2 & -\lambda_2 & E_{3/2}^{(+)} & 0 & \mathrm{i}\mu_1 & \mu_1 & 0 \\ 0 & \mu_2^* & \mathrm{i}\mu_2^* & 0 & E_{3/2}^{(-)} & \lambda_1 & \mathrm{i}\lambda_1 & 0 \\ \mu_1 & 0 & 0 & -\mathrm{i}\mu_1 & \lambda_1 & E_{1/2}^{(1)} & 0 & -\mathrm{i}\lambda_1 \\ -\mathrm{i}\mu_1 & 0 & 0 & \mu_1 & -\mathrm{i}\lambda_1 & 0 & E_{1/2}^{(1)} & \lambda_1 \\ 0 & \mathrm{i}\mu_2 & \mu_2 & 0 & 0 & \mathrm{i}\lambda_1 & \lambda_1 & E_{3/2}^{(-)} \end{bmatrix}, \tag{20}$$

where

$$\lambda_1 = \alpha_1 \cos\tfrac{1}{2}\theta, \qquad \lambda_2 = \alpha_2 \cos\tfrac{1}{2}\theta \exp i\phi, \tag{21a}$$

$$\mu_1 = \alpha_1 \sin\tfrac{1}{2}\theta, \qquad \mu_2 = \alpha_2 \sin\tfrac{1}{2}\theta \exp i\phi, \tag{21b}$$

and the energies $E^{(i)}_{1/2}$, $E^{(+)}_{3/2}$ or $E^{(-)}_{3/2}$ must now contain contributions from the corresponding diagonal elements in equation (19), e.g. in analogy with equations (5) and (6)

$$E^{(+)}_{3/2} = \tfrac{1}{2}(E^{(2)}_{3/2} - \alpha_2 + E^{(1)}_{3/2} - \alpha_1) + [\{\tfrac{1}{2}(E^{(2)}_{3/2} - \alpha_2 - E^{(1)}_{3/2} + \alpha_1)\}^2 + |V_{3/2}|^2]^{\frac{1}{2}}. \tag{22}$$

Since each of the on-diagonal 4×4 blocks in H contains interactions between degenerate or near-degenerate states, we proceed by diagonalizing these blocks exactly. The subsequent H matrix contains interactions between energetically well-separated states, and these are treated by first-order perturbation theory.

The 4×4 unitary matrix that diagonalizes the 4×4 on-diagonal blocks in equation (20) is

$$U_i = \begin{bmatrix} n_i & -\lambda_i'^* & -i\lambda_i'^* & 0 \\ \lambda_i' & n_i & 0 & -i\lambda_i'^* \\ -i\lambda_i' & 0 & n_i & \lambda_i'^* \\ 0 & -i\lambda_i' & -\lambda_i' & n_i \end{bmatrix}. \tag{23}$$

To assist in defining the quantities appearing here, we introduce the quantity

$$r_i = \tfrac{1}{2}(E^{(i)}_{1/2} - E^{(\pm)}_{3/2}) \pm [\{\tfrac{1}{2}(E^{(i)}_{1/2} - E^{(\pm)}_{3/2})\}^2 + 2|\lambda_i|^2]^{\frac{1}{2}}, \tag{24a}$$

where the upper sign is taken with $i = 2$ and the lower sign with $i = 1$. The quantities n_i and λ_i' in the matrix (23) are then given by

$$n_i = \left(1 + \frac{2|\lambda_i|^2}{r_i^2}\right)^{-\frac{1}{2}}, \qquad \lambda_i' = \frac{n_i \lambda_i}{r_i} = \frac{\lambda_i}{(r_i^2 + 2|\lambda_i|^2)^{\frac{1}{2}}}. \tag{24b,c}$$

The eigenvalues are

$$E^{(+)\prime}_{3/2} = E^{(2)}_{1/2} - r_2, \qquad E^{(-)\prime}_{3/2} = E^{(1)}_{1/2} - r_1, \tag{25a}$$

$$E^{(2)\prime}_{1/2} = E^{(+)}_{3/2} + r_2, \qquad E^{(1)\prime}_{1/2} = E^{(-)}_{3/2} + r_1. \tag{25b}$$

The effect on the elements of the off-diagonal 4×4 blocks of the transformation to the functions specified by the unitary matrices U_1 and U_2 is (provided we neglect all contributions of quadratic or higher order in α_1 and α_2) solely to multiply each element by the product $n_1 n_2$. Then, designating the eigenfunctions of H derived from first-order perturbation theory by $\Phi^{(i)}_{\pm 3/2}$ and $\Phi^{(i)}_{\pm 1/2}$, we can obtain the transformation from the original set of functions $\Lambda^{(i)}_m$ to the perturbation functions $\Phi^{(i)}_m$ as follows:

$$\begin{bmatrix} \Phi^{(2)}_{3/2} \\ \Phi^{(2)}_{1/2} \\ \Phi^{(2)}_{-1/2} \\ \Phi^{(2)}_{-3/2} \\ \Phi^{(1)}_{3/2} \\ \Phi^{(1)}_{1/2} \\ \Phi^{(1)}_{-1/2} \\ \Phi^{(1)}_{-3/2} \end{bmatrix} = \begin{bmatrix} -n_2\cos\tfrac{1}{2}\theta\exp(i\phi) & \lambda'_2 & -i\lambda'_2 & 0 & n_2\sin\tfrac{1}{2}\theta & n_1\mu_+ & -in_1\mu_+ & 0 \\ \gamma_1 & n_2 & 0 & i\gamma_1 & -\gamma_2 & 0 & 0 & -i\gamma_2 \\ i\gamma_1 & 0 & n_2 & \gamma_1 & -i\gamma_2 & 0 & 0 & -\gamma_2 \\ 0 & -i\lambda'^{*}_2 & \lambda'^{*}_2 & -n_2\cos\tfrac{1}{2}\theta\exp(-i\phi) & 0 & -in_1\mu_+ & n_1\mu_+ & n_2\sin\tfrac{1}{2}\theta \\ n_1\sin\tfrac{1}{2}\theta\exp(i\phi) & n_2\mu_- & -in_2\mu_- & 0 & n_1\cos\tfrac{1}{2}\theta & -\lambda'_1 & i\lambda'_1 & 0 \\ \gamma_3 & 0 & 0 & i\gamma^{*}_3 & \gamma_4 & n_1 & 0 & i\gamma_4 \\ i\gamma_3 & 0 & 0 & \gamma^{*}_3 & i\gamma_4 & 0 & n_1 & \gamma_4 \\ 0 & -in_2\mu^{*}_- & n_2\mu_- & n_1\sin\tfrac{1}{2}\theta\exp(-i\phi) & 0 & i\lambda'_1 & -\lambda'_1 & n_1\cos\tfrac{1}{2}\theta \end{bmatrix} \begin{bmatrix} \Lambda^{(2)}_{3/2} \\ \Lambda^{(2)}_{1/2} \\ \Lambda^{(2)}_{-1/2} \\ \Lambda^{(2)}_{-3/2} \\ \Lambda^{(1)}_{3/2} \\ \Lambda^{(1)}_{1/2} \\ \Lambda^{(1)}_{-1/2} \\ \Lambda^{(1)}_{-3/2} \end{bmatrix}, \tag{26}$$

where

$$\mu_+ = \frac{n_1 n_2 \mu_1}{E^{(+)\prime}_{3/2} - E^{(1)\prime}_{1/2}}, \qquad \mu_- = \frac{n_1 n_2 \mu_2}{E^{(-)\prime}_{3/2} - E^{(2)\prime}_{1/2}}, \tag{27a}$$

$$\gamma_1 = (\lambda'_2\cos\tfrac{1}{2}\theta - n_1\mu_-\sin\tfrac{1}{2}\theta)\exp(-i\phi), \tag{27b}$$

$$\gamma_2 = \lambda'_2\sin\tfrac{1}{2}\theta + n_1\mu_-\cos\tfrac{1}{2}\theta, \tag{27c}$$

$$\gamma_3 = (\lambda'_1\sin\tfrac{1}{2}\theta + n_2\mu_+\cos\tfrac{1}{2}\theta)\exp(i\phi), \tag{27d}$$

$$\gamma_4 = \lambda'_1\cos\tfrac{1}{2}\theta - n_2\mu_+\sin\tfrac{1}{2}\theta. \tag{27e}$$

Table 2. Calculated relative intensities of stress-induced components of transitions for Zn^- in germanium, with the impurity displaced from the tetrahedral site

The results are for transitions from a Γ_8 ground state to two Γ_8 states for $F \parallel \langle 111\rangle$. The values of the parameters N_2 and u_2 are as for Table 1 and all other symbols are defined in equations (24) and (27) of the text

Spectral line	Relative intensities of components	
	$E \parallel F$	$E \perp F$
G_3	0	$N_2(1-\frac{1}{2}u_2)\lvert\gamma_3\rvert^2$
G_4	$N_2(1-u_2)n_2^2\lvert\lambda'_2\rvert^2$	$N_2(\frac{1}{2}-\frac{1}{4}u_2)n_1^2\sin^2\frac{1}{2}\theta$ $+\frac{1}{2}N_2u_2(2n_2^2\lvert\mu_-\rvert^2+n_1n_2\lvert\mu_-\rvert\sin\frac{1}{2}\theta)$
G_1	$N_2(1+\frac{1}{2}u_2)\lvert\gamma_3\rvert^2$	0
G_2	$N_2(\frac{1}{2}+\frac{1}{2}u_2)n_1^2\sin^2\frac{1}{2}\theta$	$N_2(1-\frac{1}{2}u_2)n_2^2\lvert\mu_-\rvert^2$
D_4	$N_2(\frac{1}{2}-\frac{1}{2}u_2)n_2^2$	$\frac{1}{2}N_2u_2(n_2^2+n_2\lvert\gamma_1\rvert)+N_2(1-\frac{1}{2}u_2)\lvert\gamma_1\rvert^2$
D_3	$N_2(1-u_2)\lvert\lambda'_2\rvert^2$	$N_2(\frac{1}{2}-\frac{1}{4}u_2)n_2^2\cos^2\frac{1}{2}\theta$ $-\frac{1}{2}N_2u_2(n_2\lvert\lambda'_2\rvert\cos\frac{1}{2}\theta-2\lvert\lambda'_2\rvert^2\cos^2\frac{1}{2}\theta)$
D_2	$N_2(1+u_2)\lvert\gamma'_1\rvert^2$	$N_2(\frac{1}{2}-\frac{1}{4}u_2)n_2^2$
D_1	$N_2(\frac{1}{2}+\frac{1}{2}u_2)n_2^2\cos^2\frac{1}{2}\theta$	$N_2(1-\frac{1}{2}u_2)\lvert\lambda'_2\rvert^2$

The intensities for transitions between the ground states and G and D states are proportional to the squares of the magnitudes of the matrix elements

$$\langle\Phi^{(i)}_m \mid Q_k \mid \Lambda^{(g)}_n\rangle,$$

which, using the elements of the transformation matrix in equation (26) above, are easily expressed as linear combinations of the matrix elements $\langle\Lambda^{(i)}_l \mid Q_k \mid \Lambda^{(g)}_n\rangle$, as listed in Paper I. In tabulating these we set $N_1 = 0$, as before. The relative intensities for radiation polarized parallel and perpendicular to the stress are listed in Table 2.

(*b*) *Experimental results*

We adopt the same values for N_2, u_2 and $\theta_{3/2}$ as in Section 2. We are also able to evaluate immediately one other parameter, namely α_2, as follows. At zero stress ($F = 0$) we have $\cos(\frac{1}{2}\theta_{3/2}) = 1$ and so, from equations (21), $|\lambda_2| = |\alpha_2|$. Then using equations (24a) and (25) we obtain

$$(E^{(2)\prime}_{1/2} - E^{(+)\prime}_{3/2})_{F=0} = 2\sqrt{3}\,|\alpha_2|\,.$$

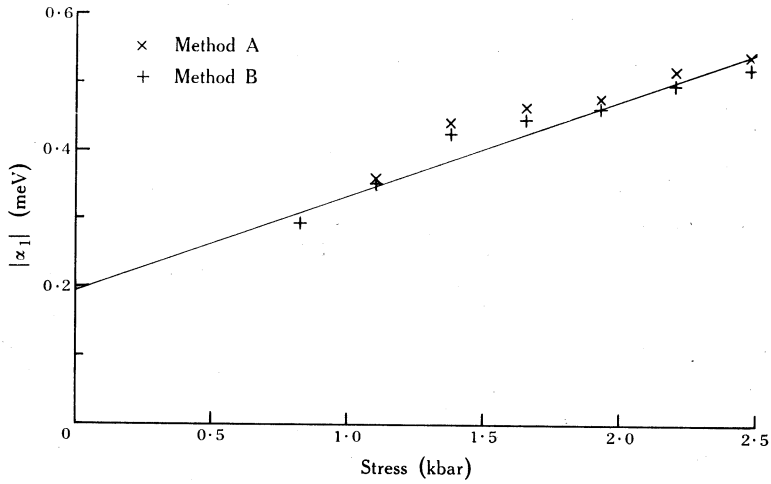

Fig. 5. Stress dependence of $|\alpha_1|$, the parameter for the G states which is proportional to the model dipole moment or to the off-centre shift. The values of $|\alpha_1|$ have been determined by two different methods using the expressions given in Table 2:

Method A, data computed from the measured intensities of the $G_3^{\perp}$ component using the known (temperature-compensated) values of N_2;

Method B, data computed from the ratios of the measured intensities of $G_3^{\perp}$ and $G_4^{\perp}$.

The D components are quite strong and their stress dependence demonstrates that there is essentially no zero-stress splitting of the D line, and thus $|\alpha_2| \approx 0$. It follows that we may take $\lambda_2 = \lambda_2' = \mu_2 = \mu_- = 0$ and then $n_2 = 1$. We note immediately that the setting of these quantities to zero predicts that the following components should be absent from the spectra: $G_3^{\parallel}$, $G_4^{\parallel}$, $D_1^{\perp}$, $D_2^{\parallel}$ and $D_3^{\parallel}$. These predictions are in agreement with the measurements, unlike the prediction of the model considered in Section 2 which, as mentioned previously, required the intensity of $G_3^{\parallel}$ to exceed the intensity of $G_3^{\perp}$.

Subject to $|\alpha_2| = 0$, the predicted intensities for $D_3^{\perp}$ and $D_4^{\perp}$ (see Table 2) are the same as those of Chandrasekhar *et al.* (1973). Thus, in this model, the intensity of $G_3^{\perp}$ is derived through the dipole-field mixing from the upper state of the G_4 component which in turn has been fed from the interaction between the upper states of the G_4 and D_3 components via the strain field, as considered above.

The intensity expression listed in Table 2 for $G_3^{\perp}$, together with simple manipulation of equations (24) and (25) to express the desired quantities in terms of measured quantities alone, allow the evaluation of $|\alpha_1|$ from the measured intensities at each stress used in the experiments. For this calculation the value of N_2 derived above, namely $16{\cdot}9\ \text{meV cm}^{-1}$, was used. The resulting value of $|\alpha_1|$ is plotted as a function

of stress in Fig. 5 (method A). For this procedure the measured intensities were compensated by the appropriate Boltzmann factors in accordance with the procedure described earlier. An alternative method for determining $|\alpha_1|$ is to use the ratio of the intensities of $G_3^{\perp}$ and $G_4^{\perp}$ at each stress. In this case no temperature compensation is needed (as both intensities are affected by the same factor), nor is the value of N_2. The points obtained for $|\alpha_1|$ as a function of stress by this second method (B) are also shown in Fig. 5.

The two methods of evaluating $|\alpha_1|$ give results in very close agreement. The small difference between them is of the same origin as the small difference between the predicted and measured intensities for $G_4^{\perp}$, shown in Fig. 3. For both sets of data we regard the point plotted at 1·38 kbar in Fig. 5 as being unusually uncertain, since the measured intensity for $G_3^{\perp}$ at this stress has been undoubtedly overestimated due to difficulties in subtracting the baseline (the tabulated intensity exceeds the intensities at each of the next two larger stress values used, and must surely be erroneous). For some of the very weak low-stress measurements, no real solution for α_1 is permitted by some of the data, but it is felt that the relative errors of measurement at these stresses are sufficiently large that no significance can be attached to this lack of success in evaluating $|\alpha_1|$.

In Fig. 5, the data for $|\alpha_1|$ as a function of stress seem to be well represented by a straight line with an intercept of about 0·2 meV and a slope such that the value of $|\alpha_1|$ increases by a factor of about 2·5 over the range of stresses used. Since α_1 is proportional to the magnitude of the dipole moment due to the off-centre movement, and this in turn is proportional to the displacement of the Zn^- from the lattice site, it appears that the displacement is mildly stress dependent, within the range of stresses used. The intercept provides an extrapolated value for $|\alpha_1|$ at zero stress which is related to a zero-stress splitting of the upper state of the G levels through

$$|E_{3/2}^{(-)\prime} - E_{1/2}^{(1)\prime}|_{F=0} = 2\sqrt{3}\,|\alpha_1|\,.$$

Thus, we predict a zero-stress splitting between the G_3 and G_4 components of $\sim$0·7 meV. Since these components are extremely weak, this is a very difficult quantity to obtain experimentally. However, if a polynomial fit is made to the energies of either the $G_3^{\perp}$ or $G_4^{\perp}$ components, the extrapolation of these fits to zero stress predicts a zero-stress position of the G line which is $\sim$0·6 meV smaller in energy than that of the observed G line. In fact, this extrapolation was used originally to predict the energy of the very weak G line before it had been observed (see Fig. 35, Butler 1974).

A calculation of the distance of off-centre movement determined from the value of α_1 is beyond the scope of this investigation, as it requires the evaluation of an appropriate matrix element using fully detailed wavefunctions. Should further experimentation confirm the zero-stress splitting of the upper state of the G line suggested here, then a calibration of α_1 in distance units would be a very useful calculation, as would a demonstration that $\alpha_2 \approx 0$.

No attempt has been made to carry the calculations through for either $\boldsymbol{F}$ parallel to $\langle 100\rangle$ or $\langle 110\rangle$. We have not carried out calculations for displacements in directions other than $\langle 100\rangle$ but it is clear from the structure of the matrix for the dipole interaction that for a $\langle 111\rangle$ displacement there is no coupling that could give rise to the G_3 component.

Acknowledgments

The authors gratefully acknowledge support from the ARGC, the University of Wollongong's Special Research Grant, the National Science Foundation (GH32001A1) and the Materials Research Laboratory Program (Nos GH33574A1 and GH33574A3).

References

Barra, F., Fisher, P., and Rodriguez, S. (1973). *Phys. Rev.* B **7**, 5285 (referred to as Paper II in the text).

Butler, N. R. (1974). Ph.D. Thesis, Purdue University.

Butler, N. R., and Fisher, P. (1976). *Phys. Rev.* B **13**, 5465 (referred to as Paper III in the text).

Chandrasekhar, H. R., Fisher, P., Ramdas, A. K., and Rodriguez, S. (1973). *Phys. Rev.* B **8**, 3836.

Chandrasekhar, H. R., Ramdas, A. K., and Rodriguez, S. (1975). *Phys. Rev.* B **12**, 5780.

Rodriguez, S., Fisher, P., and Barra, F. (1972). *Phys. Rev.* B **5**, 2219 (referred to as Paper I in the text).

Manuscript received 26 March 1979